Retroformer: Pushing the Limits of End-to-end Retrosynthesis Transformer

Yue Wan [1] **Chang-Yu Hsieh** [1] **Benben Liao** [1] **Shengyu Zhang** [1]

Abstract

Retrosynthesis prediction is one of the fundamental challenges in organic synthesis. The task is to predict the reactants given a core product. With the advancement of machine learning, computer-aided synthesis planning has gained increasing interest. Numerous methods were proposed to solve this problem with different levels of dependency on additional chemical knowledge. In this paper, we propose Retroformer, a novel Transformer-based architecture for retrosynthesis prediction without relying on any cheminformatics tools for molecule editing. Via the proposed local attention head, the model can jointly encode the molecular sequence and graph, and efficiently exchange information between the local reactive region and the global reaction context. Retroformer reaches the new state-of-the-art accuracy for the end-to-end template-free retrosynthesis, and improves over many strong baselines on better molecule and reaction validity. In addition, its generative procedure is highly interpretable and controllable. Overall, Retroformer pushes the limits of the reaction reasoning ability of deep generative models.

1. Introduction

Retrosynthesis (Corey & Cheng, 1989) is one of the major building blocks in organic synthesis, which aims to discover valid and efficient synthetic routes (i.e., reactants) given a target molecule (i.e., product). It is crucial for the pharmaceutical industry as one of the main challenges for drug discovery is to efficiently synthesize novel and complex compounds in the laboratory (Blakemore et al., 2018).

Recently, computer-aided synthesis planning has gained vast attention for its potential to save a tremendous amount of time and efforts from traditional retrosynthesis approaches. Various machine learning approaches were proposed with different levels of dependency on additional chemical knowledge. These methods can be categorized into three groups. First, template-based methods (Coley et al., 2017; Dai et al., 2019; Chen & Jung, 2021) view the retrosynthesis prediction as the template retrieval problem, where a template encodes the core reactive rule (Figure 1). After the templates are retrieved, these methods use cheminformatics tools like RDKit (rdk) to build up full reactions from the templates. Despite the state-of-the-art accuracy and guaranteed molecule validity, these methods are limited to the scope of the existing template database. In contrast, template-free methods, the second class, use deep generative models to directly generate the reactants given the product. Since molecule can be represented by both the graph and the SMILES sequence, existing approaches reframe the retrosynthesis into either sequence-to-sequence (Lin et al., 2020; Chen et al., 2019; Zheng et al., 2020; Tetko et al., 2020; Seo et al., 2021; Kim et al., 2021) or graph-to-sequence problem (Tu & Coley, 2021). These generative methods do not rely on any additional chemical knowledge and can perform chemical reasoning within a larger reaction space. The third class is semi-template-based methods, which combine the advantages of both the generative models and the prior chemical knowledge. Conventional frameworks (Yan et al., 2020; Shi et al., 2020; Somnath et al., 2020; Wang et al., 2021) in this category follow the same idea: They first identify the reactive sites and convert the product into synthons using RDKit. Then, another model completes synthons into reactants. These methods are competitive in accuracy and are interpretable by their stage-wise nature.

In this work, we are interested in the template-free generative approach for retrosynthesis prediction. Existing methods fail to fully explore the potential of deep generative model in terms of reaction reasoning, and we argue that the end-to-end Transformer-based (Vaswani et al., 2017) architecture can reach the same competitive benchmark accuracy as well as good validity and interpretability. We propose Retroformer, a novel end-to-end retrosynthesis Transformer that introduces a special attention head. It is able to jointly encode the sequential and graphical information of the molecule and allow efficient information exchange between the local reactive region and the global reaction context. The generative process is also sensitive to the exact

[1]Tencent Quantum Laboratory, Shenzhen, China. Correspondence to: Chang-Yu Hsieh <kimhsieh@tencent.com>, Shengyu Zhang <shengyzhang@tencent.com>.

Proceedings of the 39^{th} International Conference on Machine Learning, Baltimore, Maryland, USA, PMLR 162, 2022.

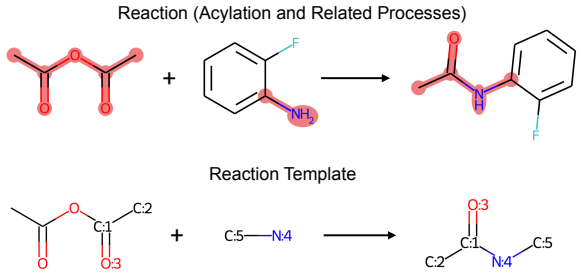

Figure 1: Sample reaction (top), reaction centers highlighted in red, which corresponds to the reaction template (bottom).

reactive region. Our end-to-end model does not rely on any additional help from cheminformatic tools for molecule editing. Experiments show that our model can improve over the vanilla Transformer by 12.5% and 14.4% top-10 accuracy in the reaction class known and unknown settings, respectively. It reaches the new state-of-the-art accuracy for template-free methods and is competitive against both template-based and semi-template-based methods. It also enjoys better molecule and reaction validity compared to strong baseline models. The model is highly interpretable and controllable for downstream usage. Our contributions are summarized as:

- We propose Retroformer, a novel Transformer-based architecture that introduces the local attention head, to push the limits of the reaction reasoning ability of deep generative models in retrosynthesis prediction.
- The proposed method reaches 64% and 53.2% top-1 accuracy for reaction class known and unknown settings, respectively, which is the new state-of-the-art performance for template-free retrosynthesis.
- The proposed method further improves the top-10 molecule and reaction validity by 23.6% and 22.0%, respectively, compared to the vanilla retrosynthesis Transformer.

2. Related Work

2.1. Retrosynthesis Prediction

Existing methods in retrosynthesis prediction can be grouped into three categories: template-based, template-free, and semi-template-based. The reaction template encodes the core reactive rules. As shown in Figure 1, a conventional template tells the potential reactive region within the molecule, as well as its potential chemical transformation. These templates are either expert-defined or automatically extracted by algorithms. In this work, we strictly differentiate the three categories by the levels of dependency on additional chemical knowledge during inference.

Template-based methods rely on an external template database. Since the template is a more efficient and interpretable representation for reactions (Heid et al., 2021; Wan et al., 2021), a large body of works (Coley et al., 2017; Dai et al., 2019; Chen & Jung, 2021) focus on capturing the reactive scores between the molecules and templates. Retrosim (Coley et al., 2017) uses molecule fingerprint similarity to rank the candidate templates. GLN (Dai et al., 2019) and LocalRetro (Chen & Jung, 2021) use graph neural network (GNN) to capture the molecule-template and atom/bond-template relationship, respectively. Despite their state-of-the-art top-k accuracy, all template-based methods suffer from the incomplete coverage issue and do not scale well.

Template-free methods, in contrast, adopt deep generative models to directly generate the reactants molecules. Besides graph, molecules can be represented using SMILES sequence. Existing works (Lin et al., 2020; Chen et al., 2019; Zheng et al., 2020; Tetko et al., 2020; Seo et al., 2021; Kim et al., 2021) take advantage of the Transformer (Vaswani et al., 2017) architecture and reframe the problem as the sequence-to-sequence translation from product to reactants. Graph2SMILES (Tu & Coley, 2021) replaces the original sequence encoder with a graph encoder to ensure the permutation invariance of SMILES. These methods rely on little additional chemical knowledge for inference. However, chemical validity can be a huge concern because validity is often not part of the training objective. Another factor comes from the ignorance of graphical structure during the sequence generation. Also, generated outcomes from beam search often suffer from the diversity issue (Vijayakumar et al., 2018), which is another practical concern for retrosynthesis.

Semi-template-based methods combine the advantage of both the generative models and additional chemical knowledge. In this work, we strictly categorize generative models which require additional help from RDKit (rdk) for molecule editing into this method group. MEGAN (Sacha et al., 2021) reframes the generative procedure as a sequence of graph edits that are completed by RDKit. In addition, most existing works (Yan et al., 2020; Shi et al., 2020; Somnath et al., 2020; Wang et al., 2021) approach the task by a two-stage procedure. Despite their architecture differences between GNN and Transformer, they follow the same idea: They first convert the product into synthons by predicting its reactive sites and performing molecule editing via RDKit, then complete the synthons into reactants by either leaving groups selection (Somnath et al., 2020), graph generation (Shi et al., 2020), or SMILES generation (Yan et al., 2020; Wang et al., 2021). Although the framework fits better with chemists' intuition of solving the problem, it brings several disadvantages. First, it requires two separate models to perform each subtask. RetroPrime (Wang et al., 2021) uses two

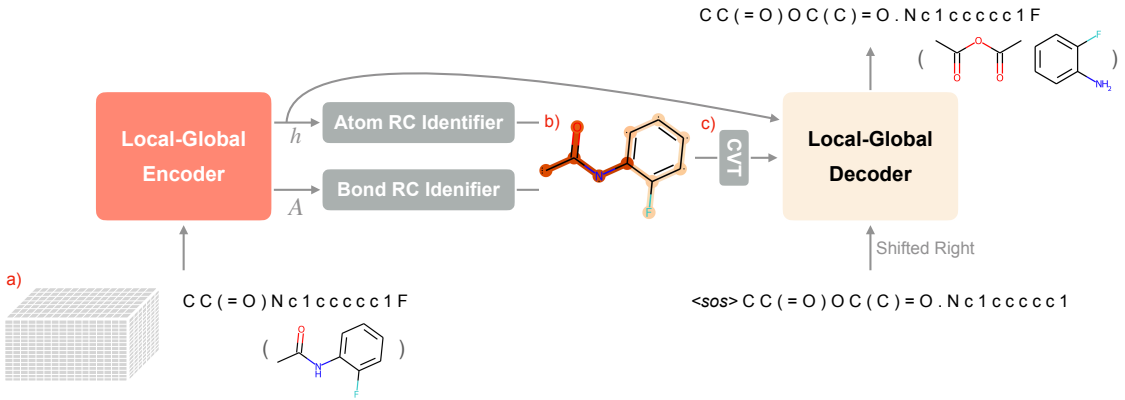

Figure 2: Architecture overview. The model takes molecular SMILES S and a) bond feature matrix A as inputs. Besides the encoder outputs h, the b) predicted reactive probability is c) converted to the indicators of S_{rc} and passed to the decoder.

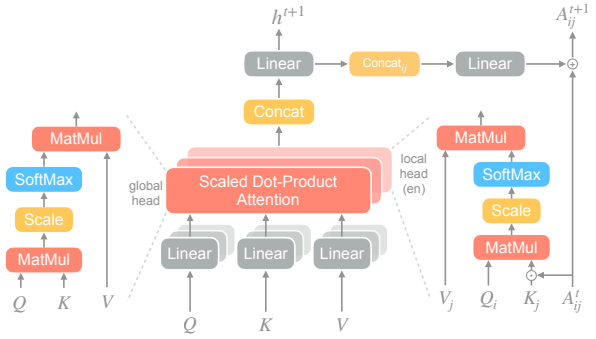

Figure 3: Local-global self-attention head in encoder.

Transformers, which doubles the computational complexity. Second, the two learning stages are independent. It means that knowledge behind reaction site prediction cannot propagate to reactants completion, which loses some chemical senses. Third, any subtle mistake from reaction site prediction will directly mislead the results. In contrast, our work attempts to walk around these disadvantages with an end-to-end Transformer while still maintaining its interpretability.

Besides different architecture designs, self-supervised molecule pretraining is also shown to be effective in retrosynthesis prediction. DMP-fusion (Zhu et al., 2021) pretrains the molecule with a dual view of SMILES and graph. Chemformer (Irwin et al., 2021) applies masked SMILES modeling to learn the molecule representation.

2.2. Graph Transformer

The introduction of Transformer into the graph domain has gained increasing interest. The global receptive fields of the self-attention and the local message passing of the graph neural network are inherently complementary and compatible. Attempts have been made in ways of incorporating graph information into the self-attention computation (Ying et al., 2021; Łukasz Maziarka et al., 2020; 2021) and integrating the conventional graph neural networks (Gilmer et al., 2017) with Transformer architecture (Dwivedi & Bresson, 2021; Chen et al., 2021).

3. Preliminary

Let $S = [s_1, s_2, ...s_n]$ be the molecular SMILES sequence with n number of tokens. Let $G_{mol} = (V_m, E_m)$ be the molecular graph. It is formed by $|V_m|$ number of atoms with $|E_m|$ number of bonds. For computation convenience, we further introduce the SMILES graph $G_{smi} = (V_s, E_s)$. V_s is made up of all the SMILES tokens, including the atom tokens (e.g., "C", "O") as well as the other special tokens (e.g., "=", "1"): $V_m \subseteq V_s = S$. In G_{smi}, the special tokens are treated as trivial nodes with no neighbors. Its edge E_s represents the graphical connections between atom tokens, which is essentially the same as bond connections E_m in G_{mol}. In general, G_{smi} is a larger but sparser graph compared to G_{mol}. The introduction of G_{smi} is merely to ensure the alignment relationship between the atoms in graph and the tokens in SMILES.

4. Retroformer

We propose Retroformer, a novel Transformer-based model that is able to perform interpretable retrosynthesis prediction in an end-to-end manner. We propose a special type of local attention head that can support efficient information exchange between the local region of reactive importance and the global reaction context. Its generative procedure is also sensitive to the exact local region. The overall training and inference can be done in an end-to-end manner. It is a fully template-free method without any additional dependency on RDKit for molecule editing. The overall architecture contains an encoder, a decoder, and two reaction center identifiers. We also propose to use SMILES alignment and on-the-fly data augmentation as two additional training strategies.

4.1. Local-Global Encoder with Edge Update

Since molecular graph can provide additional information on top of the SMILES sequence, our encoder takes both S sequence and G_{smi} (i.e., adjacency matrix and bond feature) as inputs. The bond features we considered are listed in Appendix E.1. Different from the existing graph Transformers (Ying et al., 2021; Łukasz Maziarka et al., 2020; 2021) that compute graph self-attention within the entire module, our model encodes the graph information at the head level. We specify two types of attention heads: global head and local head. The global head is the same as the vanilla self-attention head, where its receptive field is the entire SMILES sequence. The local head, on the other hand, considers the topological structure of the molecule. The receptive field of an individual token is restricted to its one-hop neighborhood, which is similar to (Zhang et al., 2021). In addition, we perform element-wise multiplication between the key vector and the edge feature to incorporate the bond information into the calculation. The roll-out form of the local head self-attention at layer l for the i^{th} token is formulated as:

$$x_i^{l+1}{}_{local} = \sum_{j \in N(i)} \sigma\left(\frac{q_i (A_{ij}^l \odot k_j)^T}{\sqrt{d}}\right) v_j \tag{1}$$
$$[q_i, k_j, v_j] = [h_i^l W^Q, h_j^l W^K, h_j^l W^V]$$

where A is the bond feature matrix, W^Q, W^K, W^V are the projection matrix for calculating query q, key k, and value v, and σ is the softmax operation. The computed representations from the global and local heads are then concatenated along the hidden dimension and passed to a linear layer, which represents the updated token features h^{l+1}. Meanwhile, the edge update module is a fully connected layer (FFN) that takes the concatenation of the updated features of the receiving and sending tokens as inputs:

$$h^{l+1} = \text{Linear}([x^{l+1}{}_{global}; x^{l+1}{}_{local}]) \tag{2}$$
$$A_{ij}^{l+1} = A_{ij}^l + \text{FFN}([h_i^{l+1}; h_j^{l+1}]) \tag{3}$$

The integration of the local, global attention heads, and the edge update module allows the model to efficiently exchange information between the local region and global molecular context. Same as the vanilla Transformer (Vaswani et al., 2017), layer normalization and residual connection are enforced between encoder layers. The final encoder outputs are the updated token representation h and the bond representation A.

4.2. Reaction Center Detection

A reaction center represents the group of atoms and bonds that are contributing factors to the chemical transformation. However, existing semi-template-based methods (Yan et al., 2020; Somnath et al., 2020; Shi et al., 2020; Wang et al., 2021) simplify this concept as the exact reactive sites. We argue that this simplification may lead to information loss of the reaction context, such as the influence of functional groups. These methods also cannot perform retrosynthesis in an end-to-end manner, since they rely on RDKit to convert the product into synthons. Instead, Retroformer predicts the reactive probability $P_{rc}(.)$ of each atom and bond and converts the reactive region of S into the attention receptive field for the decoder. In short, the detected reaction center S_{rc} is a subset of S.

Figure 2b shows a heat map visualization of the predicted reactive probability. It is done by two fully connected layers named Atom RC Identifier and Bond RC Identifier:

$$P_{rc}(s_i) = \sigma\big(\text{FFN}_{\text{atom}}(h_i)\big), s_i \in V_m \tag{4}$$
$$P_{rc}(e_{ij}) = \sigma\big(\text{FFN}_{\text{bond}}(A_{ij})\big), e_{ij} \in E_m \tag{5}$$

We will show in Section 5.3 that the learned reaction center can be easily visualized and matched with chemical heuristics. We then convert the atom and the bond reactive probability into the reactive indicator of tokens in S_{rc} by either one of the following two strategies:

- *naive*: we naively set a token as reactive if it exists in a reactive edge (i.e., $P_{rc}(e) > 0.5$) and is reactive itself (i.e., $P_{rc}(s) > 0.5$). Note that the special tokens are guaranteed to be non-reactive. This strategy is used at both training and inference stages.

- *search*: we conduct a subgraph search on the molecular graph and rank the subgraphs by their reaction center score: $\sum_{s_i \in S_{rc}} \log P_{rc}(s_i) + \sum_{s_i, s_j \in S_{rc}} \log P_{rc}(e_{ij})$. Only atoms with $P_{rc}(s) > \alpha_{atom}$ and bonds with $P_{rc}(e) > \alpha_{bond}$ are considered in the search to reduce the computational time. Detailed algorithm is described in Appendix E.4. Then, top-n subgraphs are selected as reaction center candidates. The model then generates k/n reactants for each reaction center, where k is the total number of predicted reactants. The final results are ranked by the sum of the reaction center score and the generative score. This strategy is only used at inference stage.

4.3. Local-Global Decoder

The decoder takes its generative outcomes from the previous step, the encoder outputs h, and the reaction center S_{rc} as inputs. Similar to the encoder, we also introduce two different heads in its cross-attention module. The global head is the same as the vanilla head. The local head, on the contrary, is only visible to the detected reaction center S_{rc}. It computes the sparse cross-attention instead of the

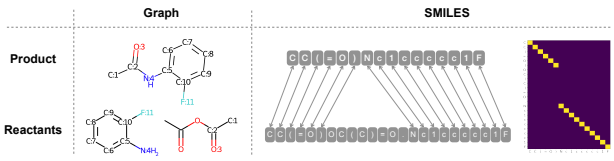

Figure 4: Token and atom alignment between product and reactants in SMILES and graph representations, respectively. The right most figure is the ground truth alignment matrix.

full cross-attention.

$$y_i^{l+1}{}_{local} = \sum_{s_j \in S_{rc}} \sigma(\frac{q_i {k_j}^T}{\sqrt{d}}) v_j \tag{6}$$
$$[q_i, k_j, v_j] = [g_i^l W^Q, h_j W^K, h_j W^V]$$

Same as the encoder, the computed representations from the global and local heads are then concatenated along the hidden dimension and passed to a linear layer, which represents the representation g^{l+1}.

$$g^{l+1} = \text{Linear}([y^{l+1}{}_{global}; y^{l+1}{}_{local}]) \tag{7}$$

It essentially converts the decoder into a conditional generative module, which is similar to the reactants generation module conditioned on the converted synthon (semi-template-based approaches). However, since S_{rc} only suggests the region of reactive importance, the condition is more relaxed than the strict condition of the converted synthon. More importantly, since Retroformer can be trained end-to-end, generative feedback can backpropagate to the reaction center learning.

4.4. SMILES Alignment

SMILES alignment is an additional learning task of Retroformer. Similar to machine translation, the SMILES sequences of the source and the target molecules are often partially aligned. A large portion of the molecules remains unchanged during the reaction. Figure 4 shows this alignment relationship in both graph and SMILES representations. The node alignment between graphs (i.e., atom mapping) can be easily converted into token alignment between SMILES. Detailed substring matching algorithm with atom-mapping is described in Appendix E.3.

Inspired by the effectiveness of the guided attention in (Deshpande & Narasimhan, 2020), we introduce the attention guidance loss between the ground truth alignment and the attention weights from the decoder's global cross-attention heads. We treat the computed cross-attention at each decoder step as a probability distribution and impose a label smoothing loss (Pereyra et al., 2017). It is a soft cross entropy loss with the label smoothing technique and is shown to be effective in classification performance. Hypothetically speaking, this guided attention can encourage the model to understand chemical reactions more efficiently.

4.5. Data Augmentation

We follow the same data augmentation tricks used in (Seo et al., 2021; Tetko et al., 2020) for the SMILES generative models, which are the SMILES permutation of the product and the order permutation of reactants. However, instead of expanding the training dataset off-the-shelf, we choose to perform the augmentation on-the-fly. At each iteration, there is a probability of 50% to permute the product SMILES and the reactants ordering. This dynamic permutation allows the model to focus more on the canonical SMILES and use the permuted SMILES for regularization. Ablation towards different augmentation methods is discussed in Appendix B.

4.6. Loss

The training schema can be viewed as an end-to-end multi-task learning. The overall loss is made up of four parts: $\mathcal{L} = \mathcal{L}_{LM} + \mathcal{L}_{RC_{bond}} + \mathcal{L}_{RC_{atom}} + \mathcal{L}_{AG}$, where $\mathcal{L}_{LM}$ is the language modeling objective, $\mathcal{L}_{RC_*}$ is the reactive probability loss, and $\mathcal{L}_{AG}$ is the SMILES alignment loss.

5. Experiments

Data We use the conventional retrosynthesis benchmark dataset USPTO-50K (Schneider et al., 2016) to evaluate our method. It contains 50016 atom-mapped reactions that are grouped into 10 reaction classes. We use the same data split as (Coley et al., 2017). We canonicalize the molecule SMILES with atom mapping following the same protocol given in (Somnath et al., 2020). We then use RDChiral (Coley et al., 2019) to extract the ground truth reaction center and use the algorithm in Appendix E.3 to extract the ground truth SMILES token alignment.

Evaluation We adopt the conventional top-k accuracy of the full reactants to evaluate the retrosynthesis performance. We also evaluate the top-k validity of the generated routes. For molecule validity, we treat a candidate as valid if RDKit (rdk) can successfully identify the molecule SMILES. The top-k validity is calculated as: $Valid(k) = \frac{1}{N \times k} \sum_1^N \sum_1^k \mathbb{1}(\text{SMILES is valid})$. We further evaluate our method with the round-trip accuracy (Schwaller et al., 2020), which is an approximation metric for reaction validity. It measures the percentage of predicted reactants that can lead back to the original product. We take the pretrained Molecule Transformer (Schwaller et al., 2019) as the oracle reaction prediction model because of its state-of-the-art performance. Our top-k round-trip accuracy calculation is slightly different from the definition adopted by RetroPrime (Wang et al., 2021) and LocalRetro (Chen & Jung, 2021): $RoundTrip(k) = \frac{1}{N \times k} \sum_1^N \sum_1^k \mathbb{1}(\text{Reach Ground Truth Product})$.

Table 1: Top-k accuracy for retrosynthesis prediction on USPTO-50K. * indicates the model with SMILES augmentation. For comparison purpose, the Aug. Transformer is evaluated without any test augmentation. Best performance is in **bold**.

Model	Top-k accuracy (%)							
	Reaction class known				Reaction class unknown			
	1	3	5	10	1	3	5	10
Template-Based								
GLN (Dai et al., 2019)	**64.2**	79.1	85.2	90.0	52.5	69.0	75.6	83.7
LocalRetro (Chen & Jung, 2021)	63.9	**86.8**	**92.4**	**96.3**	**53.4**	**77.5**	**85.9**	**92.4**
Template-Free								
Transformer	57.1	71.5	75.0	77.7	42.4	58.6	63.8	67.7
SCROP (Zheng et al., 2020)	59.0	74.8	78.1	81.1	43.7	60.0	65.2	68.7
Tied Transformer (Kim et al., 2021)	-	-	-	-	47.1	67.1	73.1	76.3
Aug. Transformer* (Tetko et al., 2020)	-	-	-	-	48.3	-	73.4	77.4
GTA* (Seo et al., 2021)	-	-	-	-	51.1	67.6	74.8	81.6
Graph2SMILES (Tu & Coley, 2021)	-	-	-	-	52.9	66.5	70.0	72.9
Retroformer$_{\text{base}}$ (Ours)	61.5	78.3	82.0	84.9	47.9	62.9	66.6	70.7
Retroformer$_{\text{aug}}$* (Ours)	**64.0**	81.8	85.4	88.3	52.9	68.2	72.5	76.4
Retroformer$_{\text{aug}}$+* (Ours)	**64.0**	**82.5**	**86.7**	**90.2**	**53.2**	**71.1**	**76.6**	**82.1**
Semi-Template-Based								
RetroXpert* (Yan et al., 2020)	62.1	75.8	78.5	80.9	50.4	61.1	62.3	63.4
G2G (Shi et al., 2020)	61.0	81.3	86.0	88.7	48.9	67.6	72.5	75.5
GraphRetro (Somnath et al., 2020)	63.9	81.5	85.2	88.1	**53.7**	68.3	72.2	75.5
RetroPrime* (Wang et al., 2021)	**64.8**	81.6	85.0	86.9	51.4	**70.8**	74.0	76.1
MEGAN (Sacha et al., 2021)	60.7	**82.0**	**87.5**	**91.6**	48.1	70.7	**78.4**	**86.1**

Table 2: Top-k SMILES validity for retrosynthesis prediction on USPTO-50K with reaction class unknown.

Model	Top-k validity (%)			
	1	3	5	10
Transformer	97.2	87.9	82.4	73.1
Graph2SMILES	**99.4**	90.9	84.9	74.9
RetroPrime	98.9	98.2	97.1	92.5
Retroformer$_{\text{aug}}$	99.3	98.5	97.2	92.6
Retroformer$_{\text{aug}}$+	99.2	**98.5**	**97.4**	**96.7**

Table 3: Top-k round-trip accuracy for retrosynthesis prediction on USPTO-50K with reaction class unknown.

Model	Top-k round-trip acc. (%)			
	1	3	5	10
Transformer	71.9	54.7	46.2	35.6
Graph2SMILES	76.7	56.0	46.4	34.9
RetroPrime	**79.6**	59.6	50.3	40.4
Retroformer$_{\text{aug}}$	78.6	71.8	**67.1**	**57.6**
Retroformer$_{\text{aug}}$+	78.9	**72.0**	**67.1**	57.2

Baseline We take GLN (Dai et al., 2019) and LocalRetro (Chen & Jung, 2021) as two strong baseline models from the *template-based* group. We take SCROP (Zheng et al., 2020), Tied Transformer (Kim et al., 2021), Augmented Transformer (Tetko et al., 2020), GTA (Seo et al., 2021), and Graph2SMILES (Tu & Coley, 2021) as the baseline models from the *template-free* group. We also train a vanilla retrosynthesis Transformer from scratch using OpenNMT (Klein et al., 2017). We take RetroXpert (Yan et al., 2020), G2G (Shi et al., 2020), GraphRetro (Somnath et al., 2020), RetroPrime (Wang et al., 2021), and MEGAN (Sacha et al., 2021) as strong *semi-template-based* baselines. We do not include the pretraining approach in the performance comparison. We experiment with three variants of the proposed model: Retroformer$_{\text{base}}$ represents the model with no data augmentation and the *naive* reaction center detection strategy; Retroformer$_{\text{aug}}$ represents the model with data augmentation and the *naive* strategy; Retroformer$_{\text{aug}}$+ represents the model with data augmentation and the *search* strategy.

Implementation Details Built on top of the vanilla Transformer (Vaswani et al., 2017), our model has 8 encoder layers and 8 decoder layers. The model is trained using the Adam optimizer (Kingma & Ba, 2017) with a fixed learning rate of $1e-4$, and a dropout rate of 0.3. The embedding dimension is set to 256, and the total amount of heads is set to 8. We split the heads by half for global and local heads. Retroformer$_{\text{base}}$ is trained on 1 NVIDIA Tesla V100 GPU for 24 hours. Our code is available at https://github.com/yuewan2/Retroformer.

Table 4: Effects of different components on retrosynthesis performance with reaction class unknown.

Settings	Modules					Top-k accuracy (%)			
	$\text{Guided}_{\text{last}}$	$\text{Guided}_{\text{all}}$	Local-global Encoder	Local-global Decoder	Reaction Center Search	1	3	5	10
(a)			$\surd$	$\surd$		45.5	60.7	65.4	69.9
(b)		$\surd$	$\surd$	$\surd$		47.0	63.1	66.9	71.1
(c)	$\surd$		$\surd$	$\surd$		47.9	62.9	66.6	70.7
(d)	$\surd$			$\surd$		44.1	60.1	64.7	70.2
(e)	$\surd$		$\surd$			46.7	63.7	68.4	73.9
(f)	$\surd$		$\surd$	$\surd$	$\surd$	**48.4**	**66.8**	**73.2**	**78.8**

Table 5: Effects of local-global encoder, reaction center search, and data augmentation on reaction center detection performance. Ablation (c) corresponds to $\text{Retroformer}_{\text{base}}$.

Settings	Top-n accuracy (%)				
	1		1	2	3
Ablation (d)	55.4	$+search$	71.6	84.1	89.9
Ablation (c)	63.0	$+search$	75.8	88.2	91.3
$\text{Retroformer}_{\text{aug}}$	67.5	$+search$	79.3	90.0	92.9

5.1. Performance

Top-k Accuracy With the reaction class known, our augmented model can achieve a 64.0% top-1 and 88.3% top-10 accuracy. It reaches the state-of-the-art performance for template-free methods and is competitive against template-based and semi-template-based methods. It improves over the vanilla retrosynthesis Transformer by 6.9% top-1 and 11.9% top-10, respectively. With the reaction class unknown, our augmented model can achieve a 52.9% top-1 and 76.4% top-10 accuracy. The top-1 accuracy reaches the state-of-the-art performance as Graph2SMILES. In addition, $\text{Retroformer}_{\text{base}}$ surpasses the vanilla retrosynthesis Transformer by a large margin in both settings. It demonstrates the promising potential for the deep generative model to perform end-to-end retrosynthesis prediction and reaction space exploration.

We further demonstrate the strength of the reaction center detection. With the top-n subgraphs proposed, $\text{Retroformer}_{\text{aug}}+$ can further boost the performance to the new state-of-the-art accuracy for template-free retrosynthesis in both experiment settings. We provide further ablation and interpretation of the $search$ strategy in Section 5.2, Section 5.3 and Appendix E.4.

Top-k SMILES Validity We take the vanilla retrosynthesis Transformer, Graph2SMILES, and RetroPrime as strong SMILES generative baselines for validity comparison with our model. We do not include template-based methods in this evaluation since molecule SMILES built from templates are guaranteed to be valid. As we mentioned before, SMILES generative models are more likely to struggle with the validity issue. Without knowing the proper reaction center, the models may modify the molecule fragments that are distant from the core reactive region, which is chemically trivial. As shown in Table 2, both of our model variants enjoy better molecule validity than others. It improves the top-10 validity over the vanilla Transformer by 23.6%. It shows that being aware of the local reactive region can encourage the model to avoid errors that propagate via the non-reactive regions.

Top-k Round-trip Accuracy To measure the reaction validity, we take the pretrained Molecule Transformer (Schwaller et al., 2019) as the oracle reaction prediction model to measure the percentage of top-k proposed synthetic routes that can lead back to the ground truth product. Table 3 shows the performance comparison of the round-trip accuracy. It shows that our method improves over the existing methods by a large margin. Our model exceeds the vanilla Transformer by 22.0% top-10 round-trip accuracy, and it also improves over RetroPrime by 12.2%. It shows that our model is more likely to propose valid and efficient synthetic routes for downstream usage.

5.2. Ablation Study

We further conduct ablation study to evaluate the effects of each component on retrosynthesis performance. As for the guided alignment loss, we experiment with two settings: $\text{Guided}_{\text{all}}$: the alignment loss is enforced at the first global heads of all decoder layers; $\text{Guided}_{\text{last}}$: the loss is enforced at the first global head of the last decoder layer.

Table 4 shows that all proposed components are necessary for $\text{Retroformer}_{\text{base}}$ to reach the best retrosynthesis performance. The improvement from (a) to (b) and (a) to (c) shows that the model can better capture the reaction knowledge from learning the SMILES alignment. We choose (c) over (b) as our final alignment loss because of its comparable performance and its lighter training duty. The 2.9% top-1 improvement from (d) to (c) indicates the effectiveness of

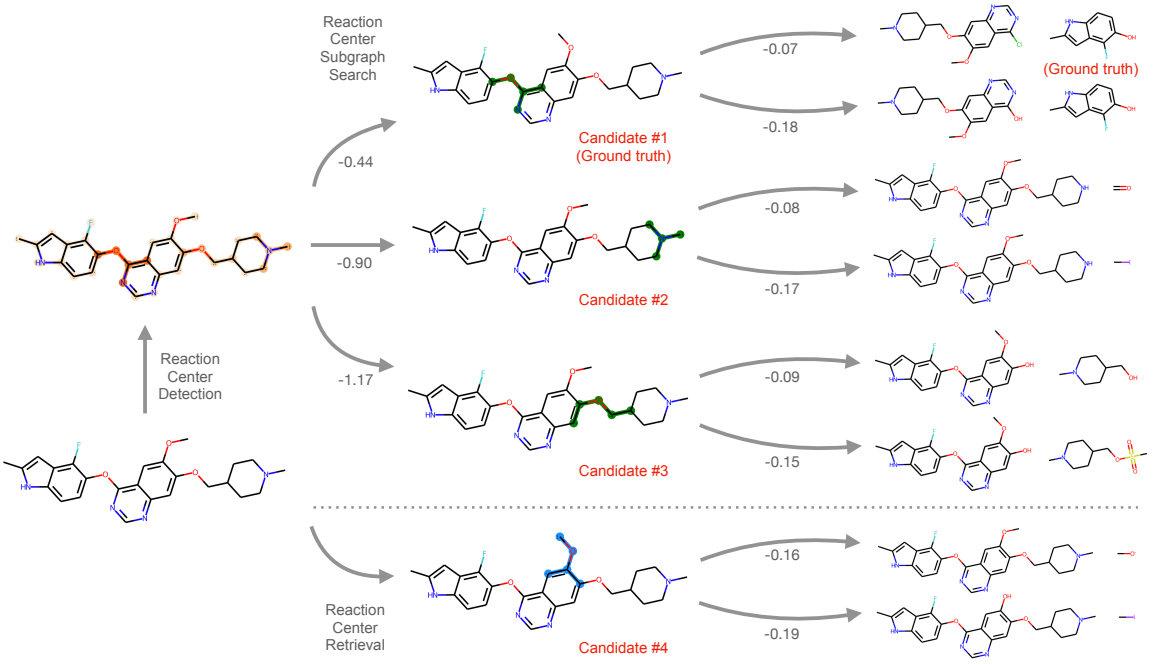

Figure 5: Retrosynthesis prediction of a randomly selected molecule.

our local-global graph Transformer encoder. Comparing (c) and (e), we could see that the local-global decoder achieves higher top-1 accuracy than the full global decoder, whereas the latter version has better top-k accuracy for $k > 1$. This is also reasonable. Focusing on a specific reaction center makes the generative process more constrained. The performance drop for $k > 1$ indicates the loss of outcome diversity. However, the local-global decoder is compatible with the reaction center search, whereas the full global decoder is not. With the $search$ strategy, the model can boost the top-k accuracy and improves the top-10 accuracy by 4.9% from (e) to (f).

In addition to the overall performance, we also evaluate the effects of the encoder structure, the proposed $search$ strategy, and the data augmentation trick on the reaction center detection top-n accuracy. As shown in Table 5, comparing (d) and (c), the local-global encoder structure improves the reaction center detection accuracy by a large margin, from 55.4% to 63%. The improvement is expected given the encoder is now aware of the graphical structure of the molecule. When the data augmentation is applied, Retroformer$_{\text{aug}}$ further improves the accuracy by 4.5% accuracy. Reaction center subgraph $search$ demonstrates its strength by its consistent improvements over all settings. We can also perform the top-n reaction center ranking rather than relying on a single candidate by the $naive$ cutoff strategy.

5.3. Qualitative Analysis

In addition to its competitive benchmark performance, Retroformer is fully interpretable and controllable by external chemical instruction.

To evaluate the interpretability and the quality of the detected reaction center, we randomly select a product molecule from the test set of USPTO-50K and predict the reactants with the $search$ strategy. We also evaluate the setting where we explicitly specify a reaction center and give it to the decoder. We term this setting as the reaction center retrieval. As shown in Figure 5, the $search$ algorithm proposes three different reaction centers (highlighted in green) given the raw reactive log probabilities. The numbers represent the reactive scores of each subgraph candidate. In this example, the top candidate matches the ground truth reaction center in the data. The third column indicates the top-2 verified predicted reactants given both the reaction center and the encoded molecule. The numbers represent the generative scores of each reactants. It shows that the model can understand the concept of reaction center and propose chemical transformations compatible with it. The outcomes from the retrieved reaction center (highlighted in blue) also demonstrate that the generation is fully controllable by external instruction (i.e., the specification of a particular reaction center). Additional analysis with respect to the learned token alignment is described in Appendix D.

6. Conclusion

We propose Retroformer, a novel Transformer-based architecture that reaches the new state-of-the-art performance for template-free retrosynthesis. With the proposed local attention heads and the incorporation of the graph information, the model is able to identify local reactive regions and generate reactants conditionally on the detected reaction center. Being aware of the reaction center also encourages the model to generate reactants with improved molecule validity, reaction validity, and interpretability. We plan to further research the multi-step template-free retrosynthesis planning problem using Retroformer as the single-step retrosynthesis prediction backbone.

References

Rdkit: Open-source cheminformatics. URL http://www.rdkit.org.

Blakemore, D. C., Castro, L., Churcher, I., Rees, D. C., Thomas, A. W., Wilson, D. M., and Wood, A. Organic synthesis provides opportunities to transform drug discovery. *Nature Chemistry*, 10(4):383–394, apr 2018. doi: 10.1038/s41557-018-0021-z. URL https://doi.org/10.1038/s41557-018-0021-z.

Chen, B., Shen, T., Jaakkola, T. S., and Barzilay, R. Learning to make generalizable and diverse predictions for retrosynthesis, 2019.

Chen, J., Zheng, S., Song, Y., Rao, J., and Yang, Y. Learning attributed graph representation with communicative message passing transformer. In Zhou, Z.-H. (ed.), *Proceedings of the Thirtieth International Joint Conference on Artificial Intelligence, IJCAI-21*, pp. 2242–2248. International Joint Conferences on Artificial Intelligence Organization, 8 2021. Main Track.

Chen, S. and Jung, Y. Deep retrosynthetic reaction prediction using local reactivity and global attention. *JACS Au*, 2021. doi: doi:10.1021/jacsau.1c00246. URL https://doi.org/10.1021/jacsau.1c00246.

Coley, C. W., Rogers, L., Green, W. H., and Jensen, K. F. Computer-assisted retrosynthesis based on molecular similarity. *ACS Central Science*, 3(12):1237–1245, nov 2017. doi: 10.1021/acscentsci.7b00355. URL https://doi.org/10.1021%2Facscentsci.7b00355.

Coley, C. W., Green, W. H., and Jensen, K. F. Rdchiral: An rdkit wrapper for handling stereochemistry in retrosynthetic template extraction and application. *Journal of Chemical Information and Modeling*, 59(6):2529–2537, 2019. doi: 10.1021/acs.jcim.9b00286. URL https://doi.org/10.1021/acs.jcim.9b00286.

Corey, E. and Cheng, X. *The Logic of Chemical Synthesis*. Wiley, 1989.

Dai, H., Li, C., Coley, C., Dai, B., and Song, L. Retrosynthesis prediction with conditional graph logic network. In *Advances in Neural Information Processing Systems*, pp. 8870–8880, 2019.

Deshpande, A. and Narasimhan, K. Guiding attention for self-supervised learning with transformers. In *Findings of the Association for Computational Linguistics: EMNLP 2020*, pp. 4676–4686, Online, November 2020. Association for Computational Linguistics. doi: 10.18653/v1/2020.findings-emnlp.419. URL https://aclanthology.org/2020.findings-emnlp.419.

Dwivedi, V. P. and Bresson, X. A generalization of transformer networks to graphs. *AAAI Workshop on Deep Learning on Graphs: Methods and Applications*, 2021.

Gilmer, J., Schoenholz, S. S., Riley, P. F., Vinyals, O., and Dahl, G. E. Neural message passing for quantum chemistry. In *Proceedings of the 34th International Conference on Machine Learning - Volume 70*, ICML'17, pp. 1263–1272. JMLR.org, 2017.

Heid, E., Liu, J., Aude, A., and Green, W. H. On the influence of template size, canonicalization and exclusivity for retrosynthesis and reaction prediction applications. *ChemRxiv*, 2021. doi: 10.33774/chemrxiv-2021-9s7gj.

Irwin, R., Dimitriadis, S., He, J., and Bjerrum, E. J. Chemformer: A pre-trained transformer for computational chemistry. *Machine Learning: Science and Technology*, 2021. URL http://iopscience.iop.org/article/10.1088/2632-2153/ac3ffb.

Kim, E., Lee, D., Kwon, Y., Park, M. S., and Choi, Y.-S. Valid, plausible, and diverse retrosynthesis using tied two-way transformers with latent variables. *Journal of Chemical Information and Modeling*, 61(1):123–133, 2021. doi: 10.1021/acs.jcim.0c01074. URL https://doi.org/10.1021/acs.jcim.0c01074. PMID: 33410697.

Kingma, D. P. and Ba, J. Adam: A method for stochastic optimization, 2017.

Klein, G., Kim, Y., Deng, Y., Senellart, J., and Rush, A. OpenNMT: Open-source toolkit for neural machine translation. In *Proceedings of ACL 2017, System Demonstrations*, pp. 67–72, Vancouver, Canada, July 2017. Association for Computational Linguistics. URL https://aclanthology.org/P17-4012.

Lin, K., Xu, Y., Pei, J., and Lai, L. Automatic retrosynthetic route planning using template-free models. *Chem. Sci.*, 11:3355–3364, 2020. doi: 10.1039/C9SC03666K. URL http://dx.doi.org/10.1039/C9SC03666K.

Pereyra, G., Tucker, G., Chorowski, J., Kaiser, L., and Hinton, G. E. Regularizing neural networks by penalizing confident output distributions. In *5th International Conference on Learning Representations, ICLR 2017, Toulon, France, April 24-26, 2017, Workshop Track Proceedings*. OpenReview.net, 2017. URL https://openreview.net/forum?id=HyhbYrGYe.

Sacha, M., Błaż, M., Byrski, P., Dabrowski-Tumański, P., Chromiński, M., Loska, R., Włodarczyk-Pruszyński, P., and Jastrzebski, S. Molecule edit graph attention network: Modeling chemical reactions as sequences of graph edits. *Journal of Chemical Information and Modeling*, 61(7):3273–3284, 2021. doi: 10.1021/acs.jcim.1c00537. URL https://doi.org/10.1021/acs.jcim.1c00537. PMID: 34251814.

Schneider, N., Stiefl, N., and Landrum, G. A. What's what: The (nearly) definitive guide to reaction role assignment. *Journal of Chemical Information and Modeling*, 56(12):2336–2346, 2016. doi: 10.1021/acs.jcim.6b00564. URL https://doi.org/10.1021/acs.jcim.6b00564. PMID: 28024398.

Schwaller, P., Laino, T., Gaudin, T., Bolgar, P., Hunter, C. A., Bekas, C., and Lee, A. A. Molecular transformer: A model for uncertainty-calibrated chemical reaction prediction. *ACS Central Science*, 5(9):1572–1583, 2019. doi: 10.1021/acscentsci.9b00576. URL https://doi.org/10.1021/acscentsci.9b00576. PMID: 31572784.

Schwaller, P., Petraglia, R., Zullo, V., Nair, V. H., Haeuselmann, R. A., Pisoni, R., Bekas, C., Iuliano, A., and Laino, T. Predicting retrosynthetic pathways using transformer-based models and a hyper-graph exploration strategy. *Chem. Sci.*, 11:3316–3325, 2020. doi: 10.1039/C9SC05704H. URL http://dx.doi.org/10.1039/C9SC05704H.

Schwaller, P., Hoover, B., Reymond, J.-L., Strobelt, H., and Laino, T. Extraction of organic chemistry grammar from unsupervised learning of chemical reactions. *Science Advances*, 7(15):eabe4166, 2021.

Seo, S.-W., Song, Y. Y., Yang, J. Y., Bae, S., Lee, H., Shin, J., Hwang, S. J., and Yang, E. Gta: Graph truncated attention for retrosynthesis. *Proceedings of the AAAI Conference on Artificial Intelligence*, 35(1):531–539, May 2021. URL https://ojs.aaai.org/index.php/AAAI/article/view/16131.

Shi, C., Xu, M., Guo, H., Zhang, M., and Tang, J. A graph to graphs framework for retrosynthesis prediction. In *Proceedings of the 37th International Conference on Machine Learning (ICML)*, pp. 8818–8827, 2020.

Somnath, V. R., Bunne, C., Coley, C. W., Krause, A., and Barzilay, R. Learning graph models for template-free retrosynthesis, 2020.

Tetko, I. V., Karpov, P., Van Deursen, R., and Godin, G. State-of-the-art augmented nlp transformer models for direct and single-step retrosynthesis. *Nature Communications*, 11 2020. doi: 10.1038/s41467-020-19266-y. URL https://doi.org/10.1038/s41467-020-19266-y.

Tu, Z. and Coley, C. W. Permutation invariant graph-to-sequence model for template-free retrosynthesis and reaction prediction, 2021.

Vaswani, A., Shazeer, N., Parmar, N., Uszkoreit, J., Jones, L., Gomez, A. N., Kaiser, L. u., and Polosukhin, I. Attention is all you need. In Guyon, I., Luxburg, U. V., Bengio, S., Wallach, H., Fergus, R., Vishwanathan, S., and Garnett, R. (eds.), *Advances in Neural Information Processing Systems*, volume 30. Curran Associates, Inc., 2017. URL https://proceedings.neurips.cc/paper/2017/file/3f5ee243547dee91fbd053c1c4a845aa-Paper.pdf.

Vijayakumar, A. K., Cogswell, M., Selvaraju, R. R., Sun, Q., Lee, S., Crandall, D., and Batra, D. Diverse beam search: Decoding diverse solutions from neural sequence models, 2018.

Wan, Y., Li, X., Wang, X., Yao, X., Liao, B., Hsieh, C.-Y., and Zhang, S. Neuraltpl: a deep learning approach for efficient reaction space exploration. *ChemRxiv*, 2021. doi: 10.26434/chemrxiv-2021-xvcwb.

Wang, X., Li, Y., Qiu, J., Chen, G., Liu, H., Liao, B., Hsieh, C.-Y., and Yao, X. Retroprime: A diverse, plausible and transformer-based method for single-step retrosynthesis predictions. *Chemical Engineering Journal*, 420:129845, 2021. ISSN 1385-8947. doi: https://doi.org/10.1016/j.cej.2021.129845. URL https://www.sciencedirect.com/science/article/pii/S1385894721014303.

Yan, C., Ding, Q., Zhao, P., Zheng, S., YANG, J., Yu, Y., and Huang, J. Retroxpert: Decompose retrosynthesis prediction like a chemist. In *Advances in Neural Information Processing Systems (NeurIPS) 33*, pp. 11248–11258. Curran Associates, Inc., 2020.

Ying, C., Cai, T., Luo, S., Zheng, S., Ke, G., He, D., Shen, Y., and Liu, T.-Y. Do transformers really perform bad for graph representation?, 2021.

Zhang, X.-C., Wu, C.-K., Yang, Z.-J., Wu, Z.-X., Yi, J.-C., Hsieh, C.-Y., Hou, T.-J., and Cao, D.-S. MG-BERT: leveraging unsupervised atomic representation

learning for molecular property prediction. *Briefings in Bioinformatics*, 22(6), 05 2021. ISSN 1477-4054. doi: 10.1093/bib/bbab152. URL https://doi.org/10.1093/bib/bbab152. bbab152.

Zheng, S., Rao, J., Zhang, Z., Xu, J., and Yang, Y. Predicting retrosynthetic reactions using self-corrected transformer neural networks. *Journal of Chemical Information and Modeling*, 60(1):47–55, 2020. doi: 10.1021/acs.jcim.9b00949. URL https://doi.org/10.1021/acs.jcim.9b00949. PMID: 31825611.

Zhu, J., Xia, Y., Qin, T., Zhou, W., Li, H., and Liu, T.-Y. Dual-view molecule pre-training, 2021.

Łukasz Maziarka, Danel, T., Mucha, S., Rataj, K., Tabor, J., and Jastrzebski, S. Molecule attention transformer, 2020.

Łukasz Maziarka, Majchrowski, D., Danel, T., Gaiński, P., Tabor, J., Podolak, I., Morkisz, P., and Jastrzebski, S. Relative molecule self-attention transformer, 2021.

A. Appendix: Validity and Round-trip Accuracy

Table 6 shows a detailed comparison between all variants of Retroformer in terms of top-k SMILES validity and round-trip accuracy. It helps to understand the effects of $search$ strategy and data augmentation alone on validity performance.

Table 6: Top-k SMILES validity and round-trip accuracy for retrosynthesis prediction with reaction class unknown.

Model	Top-k validity				Top-k round-trip acc.			
	1	3	5	10	1	3	5	10
$\text{Retroformer}_{\text{base}}$	98.4	97.0	95.4	90.5	76.4	69.4	64.2	53.6
$\text{Retroformer}_{\text{base}}+$	98.5	97.4	96.3	94.0	77.4	69.3	64.2	53.9
$\text{Retroformer}_{\text{aug}}$	99.3	98.5	97.2	92.6	78.6	71.8	67.1	57.6
$\text{Retroformer}_{\text{aug}}+$	99.2	98.5	97.4	96.7	78.9	72.0	67.1	57.2

B. Appendix: Data Augmentation

Although SMILES augmentation has become a common trick that improves over the SMILES-based molecular deep learning model, the implementation varies. Here, we perform an ablation study with our augmentation method, 2P2R_s (Seo et al., 2021), and x5M (Tetko et al., 2020). 2P2R_s represents adding an additional permuted SMILES (i.e., change the starting atom of the product and shuffle the reactants ordering) for each original SMILES into the dataset. x5M represents adding four additional permuted SMILES as well as its inverted format. The inverted format is essentially the forward reaction SMILES, with a special token added at the beginning of its string for retrosynthesis training. In our work, we apply random permutations at each training iteration instead of expanding the dataset ahead since we want the canonical form and the permuted form to be equally weighted, while still allowing the model to see various permutations. It also avoids storing a much larger dataset ahead.

Table 7 shows the performance comparison of different augmentation methods applied on Retroformer. All methods show significant performance improvement over the non-augmented setting. 2P2R_s is slightly less effective than x5M and ours, which can be explained by its small augmentation amount. Our method is slightly less effective than x5M, even though the augmentation amount from random permutation is much larger. It implies the reducing marginal improvement brought by brutally increasing the permutation amount, which is consistent with the finding in (Tetko et al., 2020). It also indicates the effectiveness of data augmentation from the forward reaction.

Table 7: Performance comparison between different data augmentation methods with reaction class unknown.

Settings	Top-k accuracy			
	1	3	5	10
None	47.9	62.9	66.6	70.7
2P2R_s	51.9	67.7	72.3	77.0
x5M	52.8	68.7	72.9	78.6
Ours	52.9	68.2	72.5	76.4

C. Appendix: Model Complexity

We measure the model complexity (i.e., total number of parameters and inference time) of Retroformer compares to other Transformer-based retrosynthesis baselines: vanilla Transformer, GTA (Seo et al., 2021), and RetroPrime (Wang et al., 2021). Note that the complexity of Augmented Transformer (Tetko et al., 2020) and Tied Transformer (Kim et al., 2021) should be roughly the same as the vanilla Transformer since they only differ by training strategies. Table 8 shows the complexity comparison measured on a NVIDIA T4 GPU with batch size equaling 8. The second column represents the vanilla Transformer based on our implementation. Its difference in inference time compared to the vanilla Transformer by OpenNMT (Klein et al., 2017) is mainly caused by the implementation difference in dataloading and beam search. It implies that Retroformer can be further sped up by efficient designs of the decoding algorithm.

Table 8: Model complexity comparison. * means the model is built by OpenNMT.

	vanilla*	vanilla	GTA*	RetroPrime*	Ours
#params	23.2M	23.2M	17.4M	75.4M	30.3M
sec/mol	0.17	0.47	0.59	2.18	0.48

D. Appendix: Qualitative Analysis, Atom Mapping

Since our model is trained to learn the token alignment between the source and the target SMILES, the predicted attention can be easily converted to atom mapping. Different from the RXNMapper (Schwaller et al., 2021) that uses an additional neighbor attention multiplier to calculate the atom mapping from the attention weights, we directly use the attention weights to do the assignment while ignoring the molecular graphical structure. Note that it does not guarantee either the one-to-one mapping from product atom to reactants atom or the equivalence of the mapped element. Figure 6(a) shows a success case of the inferred atom mapping. Figure 6(b) shows a typical failure case. This assignment mistakenly aligns [O:11] with [N:11]. The mistake is explainable since [HN:8] and [O:11] within the reactants are the exact position where chemical transformation happens. Also, this naive atom mapping fails to assign the one-to-one mapping, which is also reasonable because of the symmetry present in the second reactant.

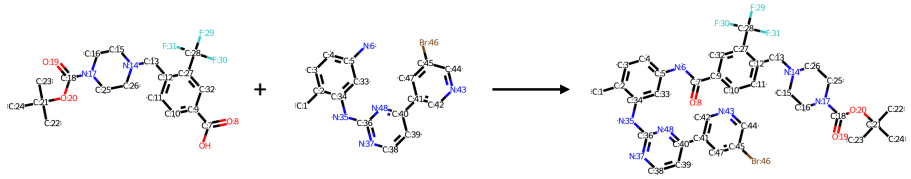

(a) Success Case

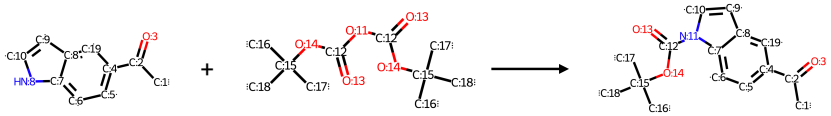

(b) Failure Case

Figure 6: Sample Atom Mapping.

E. Appendix: Implementation Details

E.1. Appendix: Bond Features

Table 9 shows the bond features considered in the proposed Retroformer, more specifically in the local-global encoder.

Table 9: Bond features.

Bond Feature	**Possible Values**	**Size**
Bond Type	Single, Aromatic, Double, Triple	4
Aromatic	True, False	1
Conjugated	True, False	1
Part of Ring	True, False	1

E.2. Appendix: SMILES Graph Construction

To ensure the alignment between the SMILES token and the atoms in graph, we expand the original molecular graph G_{mol} into the SMILES graph G_{smi} by Algorithm 1. $readSmiles()$, $getAtoms()$, $getNeighbors()$, and $writeSmiles()$ are functions supported in RDKit (rdk). The tagging procedure is to inform the connection relationship between SMILES

tokens. Rewriting the tagged SMILES without canonicalization is to ensure that the SMILES syntax does not change after the tagging.

Algorithm 1 SMILES Graph Construction

Input: molecule canonical SMILES S
Initialize V as a token list of S.
Initialize E as an empty set.
Initialize A as an empty list.
M = $readSmiles(S)$
for $a_i \in getAtoms(M)$ **do**
  Assign tag #1 to the SMILES symbol of a_i.
  for $a_j \in getNeighbors(M, a_i)$ **do**
    Assign tag #2 to the SMILES symbol of a_j.
  end for
  Get the tagged SMILES S' = $writeSmiles(M$, canonical=False)
  Retrieve the token connections $e_{(\#1,\#2)}$ by the tagged S' and add them to E.
  Retrieve the bond feature of $e_{(\#1,\#2)}$ and add them to A.
end for
Output: V, E, A

E.3. Appendix: SMILES Token Alignment Computation

The ground truth token alignment between the product SMILES and the reactants SMILES is computed as Algorithm 2. The algorithm takes the atom-mapped product and reactants as inputs. The computation works with both the canonical SMILES and the permuted SMILES.

Algorithm 2 SMILES Token Alignment Computation

Input: atom-mapped product SMILES S_p and atom-mapped reactants SMILES S_r.
Initialize the token mapping dictionary $r2s$.
for $s_{r_i} \in S_r$ **do**
  if s_{r_i} is not visited and s_r is an atom token **then**
    Locate the token s_{p_j} in S_p with the same atom mapping number as s_{r_i}: $am(s_{p_j}) == am(s_{r_i})$.
    while $s_{r_i} == s_{p_j}$ or $am(s_{p_j}) == am(s_{r_i})$ **do**
      Add alignment relationship $\{i : j\}$ into $r2s$.
      Increment i and j.
    end while
  end if
end for
for $\{i : j\} \in r2s$ **do**
  Decrement i and j.
  while $s_{r_i} == s_{p_j}$ and s_{r_i} is not an atom symbol **do**
    Add alignment relationship $\{i : j\}$ into $r2s$.
    Decrement i and j.
  end while
end for
Output: $r2s$.

E.4. Appendix: Reaction Center Subgraph Search

Algorithm 3 shows the detailed $search$ reaction center subgraph search algorithm, and Figure 7 shows a visualization of its procedure. In general, it searches for the candidate subgraphs (i.e., reaction centers) within the molecular graph via recursive pruning. It adopts a set of hyperparameters to avoid searching over the entire subgraph space.

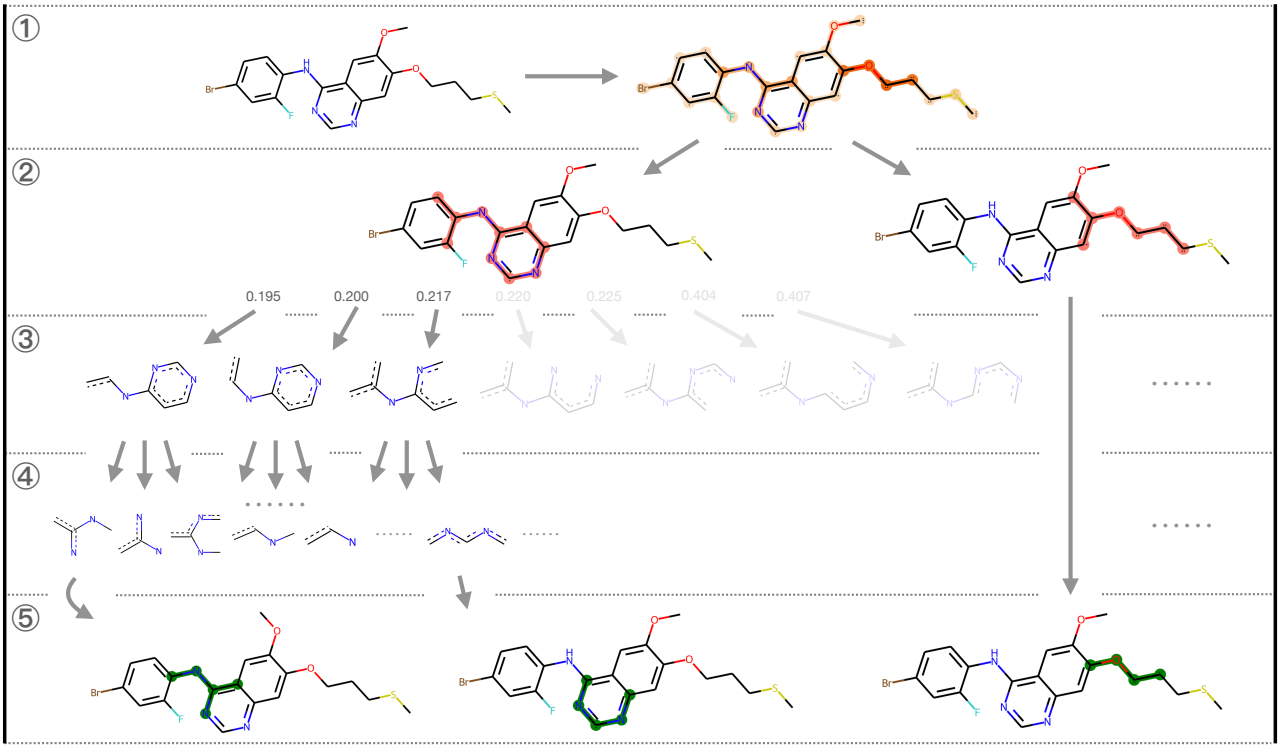

Figure 7: Visualization of the reaction center subgraph search algorithm: (1) Predict raw atom and bond reactive probability (i.e., reaction center detection); (2) Retrieve connected components based on the reactive probability; (3) Iterative pruning with $maxBranch = 3$. The number represents the reactive probability of the pruned atom; (4) Retrieve and rank all the candidate subgraphs (i.e. reaction centers); (5) Select the top-n diverse candidates from all subgraphs.

The reaction center subgraph search is done in multiple stages: First, the algorithm removes all nodes whose $P_{rc}(s_i) < \alpha_{atom}$ and edges whose $P_{rc}(e_{ij}) < \alpha_{bond}$, and retrieves all the connected components C from the edited graph. Second, for each connected component $c = (V_c, E_c)$, the algorithm retrieves all its subgraphs and the corresponding reactive scores via recursive pruning. The recursive pruning takes $maxRootSize, minLeafSize, maxBranch$ as three arguments to control its search space. If the number of nodes $|V_c|$ is larger than $maxRootSize$, then the algorithm directly removes $|V_c| - maxRootSize$ number of nodes with the lowest reactive scores. At each iteration, the algorithm considers nodes that lie along the border of the current graph as pruning candidates to ensure that the pruned graph is still a connected graph. $maxBranch$ is the maximum branching factor of the recursive pruning. The algorithm first ranks the pruning candidates by their atom reactive probability, and keeps only the top-$maxBranch$ candidates for pruning. The recursion stops when $|V_c| = minLeafSize$. After all subgraphs are retrieved from a root connected component c, we rank them by their reactive scores. Prior to the overall subgraph ranking, we remove all subgraphs (excluding the top-1 subgraph) that share at least two common nodes with the top-1 subgraph to ensure the candidates' diversity. At last, we gather the remaining subgraphs from all the root connected components C and retrieve the top-n reaction center candidates by their reactive scores.

In our experiments, we set $n = 3$. Note that it only guarantees the maximum amount of reaction center candidates. We set the temperature $T = 10$ to flatten the reactive probabilities $P_{rc}(s)$ and $P_{rc}(e)$. As for α_{atom} and α_{bond}, instead of having a fixed value, we dynamically set the two parameters as the k_s^{th} and k_e^{th} percentile of $P_{rc}(s)$ and $P_{rc}(e)$, respectively. Based on the best validation performance, we set $k_s = 40, k_e = 40$ for reaction class unknown setting, and $k_s = 40, k_e = 55$ for reaction class known setting; β is the parameter that controls the $minLeafSize$. For simplicity reason, we set $\beta = 0.5, maxRootSize = 25$, and $maxBranch = 5$.

The exact reactive score for a candidate subgraph $G = (V, E)$ is computed as follow:

Algorithm 3 Reaction Center Subgraph Search

Input: $P_{rc}(s), P_{rc}(e), G_{smi}, \alpha_{atom}, \alpha_{bond}, \beta$.
Remove all nodes whose $P_{rc}(s_i) < \alpha_{atom}$ from G_{smi}.
Remove all edges whose $P_{rc}(e_{ij}) < \alpha_{bond}$ from G_{smi}.
Retrieve all the connected components C from the edited SMILES graph.
for $c = (V_c, E_c) \in C$ **do**
  Set $maxRootSize = 25$.
  Set $maxBranch = 5$.
  Set $minLeafSize = \sum_{s_i \in c} \mathbb{1}(P_{rc}(s_i) > \beta)$, where $s_i \in c$.
  if $|V_c| > maxRootSize$ **then**
    Remove $|V_c| - maxRootSize$ nodes with the lowest $P_{rc}(s_i)$.
  end if
  Retrieve all subgraphs of c (with scores) via recursive pruning with $maxBranch$ and $minLeafSize$.
  Remove all subgraphs who share more than two common nodes with the top-1 subgraph.
end for
Output: Subgraphs with reactive scores.

$$\frac{1+\varphi(|V|,\mu,\sigma^2)}{M}\Big(\sum_{s_i\in V}\log P_{rc}(s_i)+\sum_{e_{ij}\in E}\log P_{rc}(e_{ij})\Big) \tag{8}$$

where $M = |V| + |E|$ is the normalization factor, and $\varphi(.)$ is the density function of a normal distribution of the size of reaction centers. We set $\mu = 5.55$ and $\sigma = 1.2$, which are computed from the training dataset. This is a heuristic factor taken from the observation that the size of the reaction centers has little relationship with the size of the molecule, but is rather normally distributed (Figure 8).

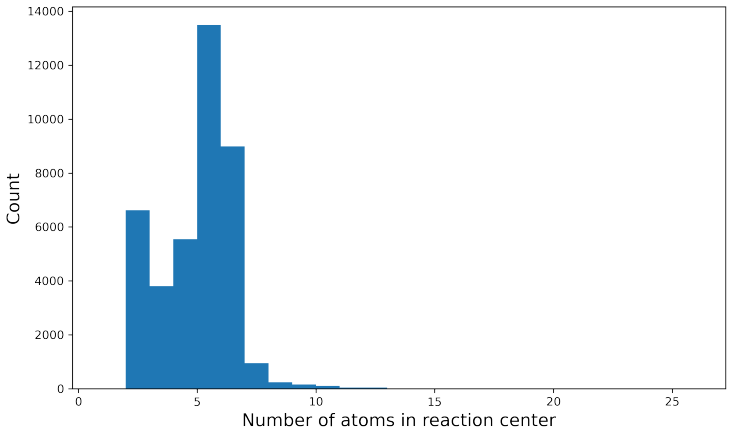

Figure 8: Histogram of the size of reaction centers in the training set of USPTO-50K.